Phase-matching and nonlinear optical processes in silicon waveguides

D. Dimitropoulos, V. Raghunathan, R. Claps, and B. Jalali

Optoelectronic Circuit and Systems Laboratory
Department of Electrical Engineering
University of California, Los Angeles CA90095-1594
jalali@ucla..edu

http://www.ee.ucla.edu/~oecs/

Abstract: The efficiency of four-wave-mixing arising from Raman and non-resonant nonlinear susceptibilities in silicon waveguides is studied in the $1.3 - 1.8\mu m$ regime. The wavelength conversion efficiency is dominated by the Raman contribution to the nonlinear susceptibility, and high conversion efficiencies can be achieved under the phase-matching condition. In this context, dispersion in silicon waveguides is analyzed and it is shown that phase-matching is achieved in properly engineered waveguides where birefringence compensates for material dispersion. Finally the sensitivity of the phase mismatch to fabrication-induced errors in waveguide dimensions is quantified.

References and links

1. B. Jalali, S. Yegnanarayanan, T. Yoon, T. Yoshimoto, I. Rendina, F. Coppinger, "Advances in Silicon-on-Insulator Optoelectronics," IEEE J. Sel. Top. Quantum Electron. **4**, 938 – 947 (1998).
2. M. Loncar, T. Doll, J. Vuckovic, A. Scherer, "Design and fabrication of silicon photonic crystal optical waveguides," J. Lightwave Technol. **18**, 1402-1411 (2000).
3. R. Claps, D. Dimitropoulos, V. Raghunathan, Y. Han, B. Jalali, "Observation of stimulated Raman amplification in silicon waveguides," Opt. Express **11,** 1731-1739 (2003), http://www.opticsexpress.org/abstract.cfm?URI=OPEX-11-15-1731.
4. R. Claps, V. Raghunathan, D. Dimitropoulos, B. Jalali, "Anti-Stokes Raman conversion in Silicon waveguides," Opt. Express **11,** 2862-2872 (2003), http://www.opticsexpress.org/abstract.cfm?URI=OPEX-11-22-2862.
5. S.S. Jha, N. Bloembergen, "Nonlinear Optical Susceptibilities in Group-IV and III-V semiconductors," Phys. Rev. **171**, 891 – 898 (1968).
6. R. Loudon, "Theory of first-order Raman effect in crystals," Proc. Roy. Soc. (London) A **275**, 218 – 232 (1963).
7. J.J. Wynne, "Optical Third-Order Mixing in GaAs, Ge, Si, and InAs," Phys. Rev. **178**, 1295 – 1303 (1969).
8. D. Dimitropoulos, B. Houshmand, R. Claps, B. Jalali, "Coupled-mode theory of the Raman effect in Silicon-On-Insulator waveguides," Opt. Lett. **28**, 1-3 (2003).
9. H.K. Tsang, C.S. Wong, T.K. Liang, I.E. Day, S.W. Roberts, A. Harpin, J. Drake, M. Asghari, "Optical dispersion, two-photon absorption and self-phase-modulation in silicon waveguides at $1.54\mu m$ wavelength," Appl. Phys. Lett. **80**, 416 – 418 (2002).
10. M. Dinu, F. Quochi, H. Garcia, "Third-order nonlinearities in silicon at telecom wavelengths," Appl. Phys. Lett. **82** , 2954 – 2956 (2003).
11. E. Golovchenko, P.V. Mamyshev, A.N. Pilipetskii, E.M. Dianov, "Mutual Influence of the Parametric Effects and Stimulated Raman Scattering in Optical Fibers," IEEE J. Quantum Electron. **26**(10) p.1815-1820 (1990).
12. R.A. Soref, J. Schmidtchen, K. Petermann, "Large single-mode rib waveguides in GeSi-Si and Si-on-SiO₂," IEEE J. Quantum Electron. **27**, 1971 – 1974 (1991).

13. H.H. Li, "Refractive index of silicon and germanium and its wavelength and temperature derivatives," J. of Phys. & Chem. Ref. Data, 9, p.591-658 (1980).

14. G.P. Agrawal, *Nonlinear Fiber Optics*, (Academic Press, San Diego, 2001) ISBN 0-12-045143-3.

15. Intel Technology Journal, Vol. 06 (02), ISSN 1535-766X. http://www.intel.com/technology/itj/2002/volume06issue02/art01_130nmlogic/p01_abstract.htm

1. Introduction

Silicon-On-insulator (SOI) has emerged as an ideal platform for integrated optics. Driven by the electronic IC industry, the quality of commercial SOI wafers continue to improve while the cost continues to decrease. This along with complete compatibility with silicon IC technology has been fueling interest in SOI integrated optics [1]. Compared to other integrated optics platforms, a distinguishing property of SOI is the tight optical confinement made possible by the large index mismatch between the silicon and SiO_2. This renders SOI ideal for photonic band structures as it minimizes radiation into the substrate even when extreme index modulation is performed [2]. While a myriad of high performance passive devices have been realized, creation of active devices has been an elusive goal. In particular, the near-absence of nonlinear optical properties caused by the inversion symmetry of the crystal structure, and the lack of efficient optical transitions due to the indirect band structure, have contributed to the premature perception of silicon being useful only as an optically passive material.

Recently, we have proposed and demonstrated the use of Raman effect to achieve active optical functionality in silicon waveguides [3]. Raman effect is successfully exploited in fiber amplifiers and lasers, however several kilometers of fiber are required to create a device. The premise is that the gain coefficient for Stimulated Raman Scattering (SRS) is approximately 10^4 times higher in silicon than in silica. Additionally, SOI waveguides can confine the optical field to an area that is approximately 100 times smaller than the modal area in a silica fiber. The combination of these properties will make SRS observable over millimeter-scale interaction lengths encountered in an integrated optic device.

The observation of SRS has led to the first demonstration of wavelength conversion in silicon waveguides [4]. The conversion is achieved by the combination of SRS and the parametric 3rd order optical nonlinearity in the medium. Coherent Anti-Stokes Raman Scattering (CARS) occurs through coherent interaction of the two waves with a high intensity pump. Wavelength conversion is of paramount importance in optical networks because it enables optical packet switching, a key milestone in the realization of all-optical networks. While the recent demonstration [4] highlights the potential for a silicon wavelength converter, the observed conversion efficiency of 10^{-5} will have to be drastically increased before a practical device can be realized. Since the limited efficiency is due to the phase mismatch inside the SOI rib waveguide, the key problem is how to engineer the Group Velocity Dispersion (GVD) inside the waveguide in order to attain phase matching.

In this paper, we outline this problem and propose an effective solution leading to high conversion efficiencies. Through numerical simulations, we show how phase matching can be achieved by the proper design of the rib geometry. The analysis takes into account contributions due to (i) material dispersion, (ii) waveguide dispersion, (iii) self and cross phase modulation, and (iv) birefringence. The two dominant terms, material and birefringence, can offset each other leading to ideal phase matching. It is shown that in such waveguides, peak conversion efficiencies of tens of percent can be achieved at pump intensities of $10MW/cm^2$ in a 2cm long waveguide with a loss of 1dB/cm. In Section 2, the relevant nonlinear optical properties of silicon are summarized. Section 3 outlines the phase matching condition and describes various contributions to the overall GVD. Section 4 provides the design of phase matched SOI waveguides. Section 5 considers the sensitivity of phase matching to variations in waveguide dimension caused by fabrication errors.

2. Non-linear processes in SOI waveguides

In silicon there are two main sources of 3rd order nonlinear optical response. The nonlinear response of the electrons to the optical field (electronic – non-resonant susceptibility) [5], and the interaction of the optical field with the optical branch of the lattice vibration through the electron-phonon interaction (Raman – resonant susceptibility) [6]. For the Raman interaction the Stokes shift is $\Omega_R = 15.6$THz and the resonance half-width is $\Gamma_R = 2\pi \times 53$GHz. In the crystallographic axes system x,y,z the resonant susceptibility has nonzero components $\chi_{xyyx}^{R} = \chi_{xyxy}^{R}$ (and other permutations of the cubic axes x,y,z) and these can be written as :

$$\chi_{ijkl}^{R}(-\omega_1 \mp \Delta\omega, \omega_1 \pm \Delta\omega, -\omega_1, \omega_1) = \frac{2\Omega_R \Gamma_R \xi_R}{2j\Gamma_R \Delta\omega + \Omega_R^2 - (\Delta\omega)^2} \qquad (1)$$

where $\Delta\omega$ is the frequency shift with respect to the pump frequency and the peak value ($\Delta\omega = \Omega_R$) is $\chi_{xyyx}^{R} = -j\xi_R = -j11.2\times10^{-18}$ (m^{2}V^{-2}). For comparison, the other contribution to the 3rd order nonlinear susceptibility, i.e., the electronic (non-resonant) susceptibility in silicon is $\chi_{xyyx}^{NR} = 0.25\times10^{-18}$ with $\chi_{xyyx}^{NR} = \chi_{xyxy}^{NR} = \chi_{xxyy}^{NR} \approx 0.5\chi_{xxxx}^{NR}$ [7]. Two-photon absorption will be ignored throughout the paper. It has been measured in previous work [3] and found to be negligible for intensities up to ~ 100MW/cm^2.

The situation described above is for a bulk crystal. We have recently shown that in SOI waveguides the resonant part of the nonlinear optical constants are modified by a scaling factor which is very close to unity and that TE and TM Stokes waves generated by Stimulated Raman Scattering (SRS) propagate independently [8]. Also measurement in [9] for SOI waveguides at 1.54 μm have yielded a non-resonant susceptibility of $\chi_{xxxx}^{NR} = 0.39\times10^{-18}$, which is very close to the value reported for bulk silicon in [7,10].

CARS involves three waves at frequencies $\omega_1, \omega_2 = \omega_1 - \Omega + \Delta\omega_2$, and $\omega_3 = \omega_1 + \Omega + \Delta\omega_3$, where the optical power of first wave is much higher than the power in the other two. It is understood that frequency deviations from resonance, $\Delta\omega_2, \Delta\omega_3$ are smaller than the half-width Γ_R. More specifically the amplitude conversion efficiency between the Anti-Stokes and Stokes waves are [11]

$$C_{AS \to S} = \kappa_{23}e^{\kappa_{23}x}\frac{e^{s^- x} - e^{s^+ x}}{s^- - s^+}, \qquad C_{S \to AS} = -\kappa_{32}e^{-\kappa_{33}x}\frac{e^{\lambda^- x} - e^{\lambda^+ x}}{\lambda^- - \lambda^+} \qquad (2)$$

where

$$\lambda = s^{\pm} - j\Delta\beta + \kappa_{22} + \kappa_{33}$$

$$s^{\pm} = \frac{j\Delta\beta - \kappa_{22} - \kappa_{33} \pm \sqrt{(j\Delta\beta - \kappa_{22} - \kappa_{33})^2 - 4\kappa_{23}\kappa_{32}}}{2} \qquad (3)$$

$$\kappa_{22} = j\frac{k_2^2}{2\beta_2}\chi^R |A_1|^2, \qquad \kappa_{23} = j\frac{k_3^2}{2\beta_2}(2\chi^{NR} + \chi^R)A_1^2$$

$$\kappa_{33} = j\frac{k_3^2}{2\beta_3}\chi^R \mid A_1 \mid^2 , \qquad \kappa_{32} = j\frac{k_2^2}{2\beta_3}\left(2\chi^{NR} + \chi^R\right)(A_1*)^2 \qquad (4)$$

In the above equations x is the propagation length [11] and $\Delta\beta$ is the phase mismatch (to be formally defined later). The importance of phase-matching lies in the fact that the conversion efficiency between the two-waves varies as $\sim \sin c^2(\Delta\beta x/2)$ when $\Delta\beta >> \kappa_{22}, \kappa_{33}$ as can be seen from Eq. (2). Referring to Equation (4), since $\mid \chi^R \mid / \mid \chi^{NR} \mid \sim 45$, the conversion efficiency is dominated by the Raman contribution to the nonlinear susceptibility.

The effect of the SPM of the pump wave and of the XPM of the Stokes and Anti-Stokes waves due to the pump wave are included in the $\Delta\beta$ term, as will be shown below. The efficiency for Stokes to anti-Stokes power conversion is plotted in Fig. 1 for a 2cm long waveguide with $4\mu m^2$ cross-section and for 400mW monochromatic pump at 1434nm. 0.1 and 1 dB/cm losses have been assumed in this example. A peak efficiency of ~18% is obtained at the phase matched condition. It shows that the conversion efficiency is a strong function of phase mismatch. For example even a modest phase mismatch of 10 cm^{-1} reduces the conversion efficiency by approximately 20dB. It should be acknowledged that this analysis assumes a zero linewidth pump. The finite pump linewidth will lower the overall efficiency.
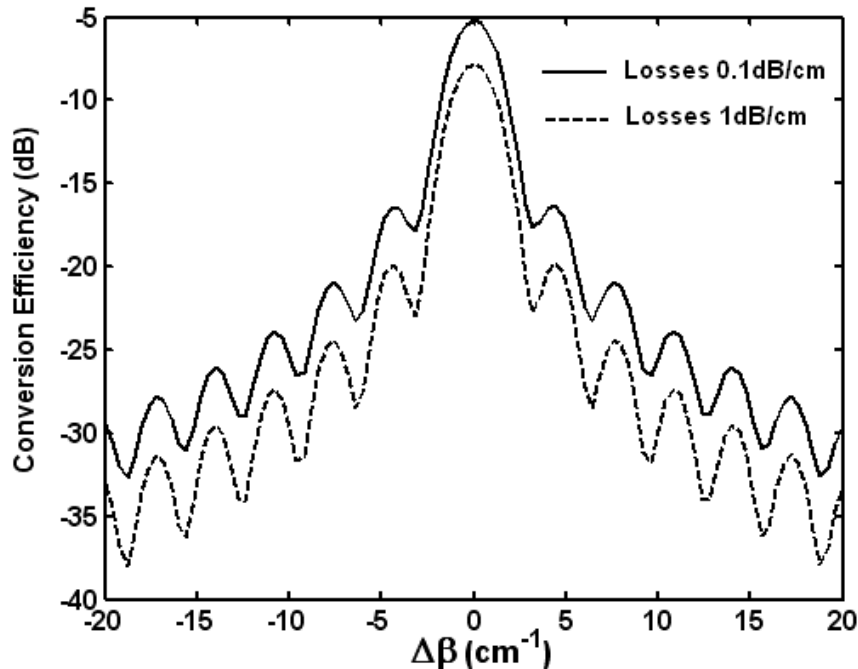

Fig. 1. Conversion efficiency in a 2cm waveguide at 10MW/cm^2 pump intensity with linear losses 0.1 dB/cm (solid line) and 1dB/cm (dashed line). Stokes to Anti-Stokes efficiency is shown for pump centered at 1434nm.

3. The phase-matching condition in SOI waveguides

The SOI rib waveguide geometry is shown in Fig.2. It has been shown [12] that single-mode propagation can be realized through a judicious choice of w and h, even for a wavelength $\lambda << w, h$. When the single-mode condition is satisfied the waveguides support two modes, one approximately TE polarized (E field parallel to the horizontal) and the other approximately TM polarized (H field parallel to the vertical). Since the index difference between Si and SiO$_2$ is large, the mode lies almost entirely in the Si area and we expect the dispersion of these waveguides to be very low.
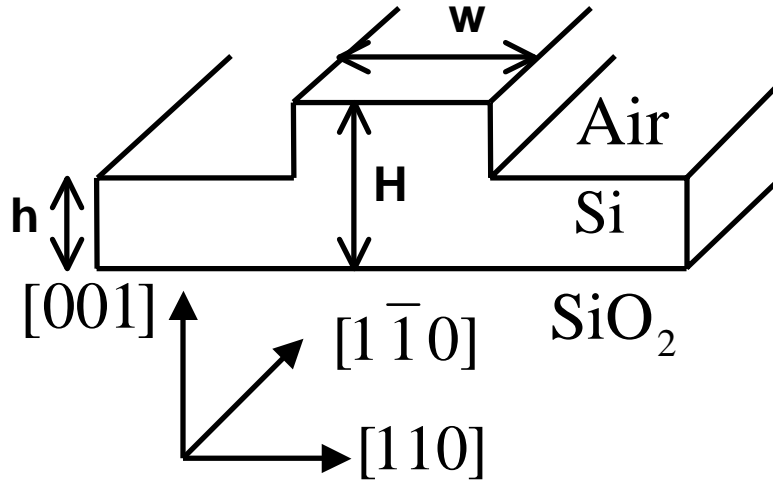
Fig. 2. SOI rib waveguide geometry.

The phase-mismatch of the three waves is defined as

$$\Delta\beta = 2\beta(\omega_1) - \beta(\omega_2) - \beta(\omega_3) \qquad (5)$$

and can be written with respect to factors that contribute to it as

$$\Delta\beta = \Delta\beta_B + \Delta\beta_{WD} + \Delta\beta_{MAT} + \Delta\beta_{SPM,XPM} \qquad (6)$$

The various contributions the phase-mismatch admits are: $\Delta\beta_B$ induced by the waveguide birefringence, $\Delta\beta_{WD}$ induced by the waveguide dispersion, $\Delta\beta_{MAT}$ induced by the material dispersion, and $\Delta\beta_{SPM,XPM}$ is induced by the self-phase modulation of the pump wave at ω_1 and the cross-phase modulation of the sidebands due to the pump wave. In the normal dispersion regime of the material $\Delta\beta_{MAT} < 0$ and in the anomalous regime $\Delta\beta_{MAT} > 0$. $\Delta\beta_{SPM,XPM} < 0$, when the nonlinear susceptibility has positive sign, as is the case in silicon. The birefringence contribution can be positive or negative depending on the relative polarization of the sidebands with respect to the pump.

The phase-matching technique to be used depends on the material dispersion region. For example, in single-mode fiber in the 1550nm region, one can phase-match the waves by either

increasing the pump power and thus increasing the negative term $\Delta\beta_{SPM,XPM}$, or if the fiber is polarization maintaining, one can launch the waves such that ω_2, ω_3 are on the slow axis and $\Delta\beta_B < 0$.

Let's now consider the CARS in SOI waveguides. We assume TE polarized pump, TM polarized Stokes and Anti-Stokes waves and $\Delta\omega_2 = \Delta\omega_3 = 0$. Since the optical fields have frequencies below the bandgap of silicon, the dispersion is normal $\left(d^2\beta/d\omega^2\right)_{MAT} > 0$.

We assume the refractive index is isotropic and model the material dispersion using the Sellmeier model of Li [13] :

$$n^2 = \varepsilon_1 + \frac{A}{\lambda^2} + \frac{B\lambda_1^2}{\lambda^2 - \lambda_1^2} \tag{7}$$

where $\varepsilon_1 = 11.6858$, $A = 0.939816$, $B = 8.10461 \times 10^{-3}$ and $\lambda_1 = 1.1071\mu m$. The third term is the contribution of the indirect bandgap and the first two represent contributions from all other resonances. The wavevector mismatch that this dispersion contributes with respect to the pump wavelength is shown in Fig. 3. For comparison, the material GVD induced mismatch for silica fiber is also shown. The model used for fiber is the three resonance Sellmeier model in [14].

In our region of interest (pump wavelengths larger than 1.4μm) considering only the 2nd order material dispersion is sufficient and $\Delta\beta_{MAT} \approx -\left(\dfrac{d^2\beta}{d\omega^2}\right)_{MAT} \Omega^2 < 0$. From Fig. 3 we can see that the dispersion that we have to compensate is a very large value, on the order of $-110\,cm^{-1}$. As a side note, while in fiber the material dispersion is much lower than in silicon, this does not mean that phase matching is easier for the CARS. As can be seen from Eqs. (2) and (3) the regime for which the conversion efficiencies are particularly high are for $\Delta\beta/\operatorname{Im}(\kappa_{22} + \kappa_{33}) \sim 1$. Thus, because in fiber the Raman susceptibility is much lower than silicon, the condition for phase-matching is more stringent in fiber.

The waveguide dispersion was obtained from numerical simulations (next section). The value is positive but is in the range $\sim 5 - 15\,cm^{-1}$. Hence it is insufficient for compensating for the material dispersion. Because the non-resonant susceptibility of silicon is very small, SPM and XPM contributions to $\Delta\beta$ are negligible. Indeed, $\Delta\beta_{SPM,XPM} = -\dfrac{\pi}{cn^2\varepsilon_o\lambda_1}\chi^{NR}I_1$, where I_1 is the pump intensity and χ^{NR} the non-resonant susceptibility. Even for intensities of the order of $100MW/cm^2$, the nonlinear contribution to the phase mismatch is $\Delta\beta_{SPM,XPM} \sim -0.2cm^{-1}$, a negligible value.

In SOI rib waveguides $\beta_{TE}(\omega_1) > \beta_{TM}(\omega_1)$ and for the polarizations configuration in the experiments of Reference [4] $\Delta\beta_B > 0$. As simulations in the next section reveal, for this configuration, this term is positive and is in the range of $50 - 600\,cm^{-1}$, depending on the specific rib dimensions. Thus the birefringence can be used to cancel the material dispersion and phase-match the interacting waves. Should one use TM polarization for the pump and TM for the Stokes and Anti-Stokes waves, the birefringence term will have the opposite sign and it adds up to the material dispersion.

Ignoring the XPM/SPM contribution and expanding the propagation constants in a Taylor series around the pump frequency ω_1 , the phase mismatch in Eq. (5) can be written as:

$$\Delta\beta \approx 2(\beta_{TE}(\omega_1) - \beta_{TM}(\omega_1)) - \left(\frac{d^2\beta_{TM}}{d\omega^2}\right)_{WG+MAT} \Omega^2 \qquad (8)$$

From left to right, the terms are due to birefringence, waveguide dispersion and material dispersion, respectively. For non-zero $\Delta\omega_2, \Delta\omega_3$ the added contribution to the above expression is (to 1st order in $\Delta\omega_2 , \Delta\omega_3$):

$$-\left(\frac{d\beta_{TM}}{d\omega}\right)_{WG+MAT} (\Delta\omega_2 + \Delta\omega_3) + \left(\frac{d^2\beta_{TM}}{d\omega^2}\right)_{WG+MAT} \Omega(\Delta\omega_2 - \Delta\omega_3) \quad (9)$$
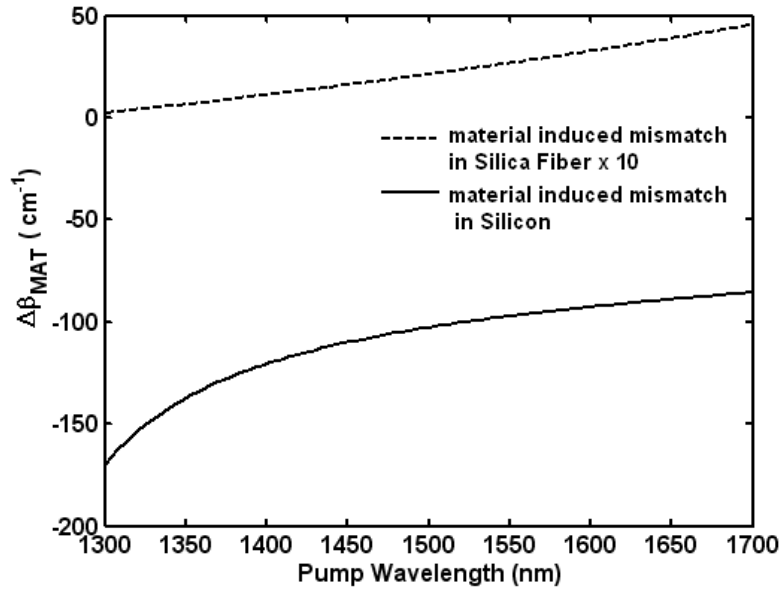
Fig. 3. Material induced wavevector mismatch with respect to the pump wavelength for the CARS process. Both the case of silicon (solid line) and the case of fiber (dashed line) are shown for comparison.

It is thus possible, to achieve phase-matching by designing the waveguide so that the birefringence and material dispersion terms cancel each other.

4. Simulation results

The waveguide dispersion and birefringence effects were calculated with a commercial software package (Fimmwave^{TM} Version 4.1.6) which uses the mode-matching technique to calculate the propagation constant. All the waveguides chosen for the simulations satisfy the single-mode condition [12]. First a fixed total rib height H = 1.4um was chosen and the ratio h/H was varied from 0.5 to 0.7, with the rib width w taking values 1.0 , 1.2 and 1.4μm. The results for the total wavevector mismatch in CARS are shown in Figs. 4 and 5, for anti-Stokes (1334.8nm) to Stokes (1550nm) conversion and Stokes (1847.9 nm) to Anti-Stokes (1550nm)

respectively. The mismatch is different in the two cases because the wavelengths involved are different. Larger pump wavelength leads to higher birefringence and waveguide dispersion.
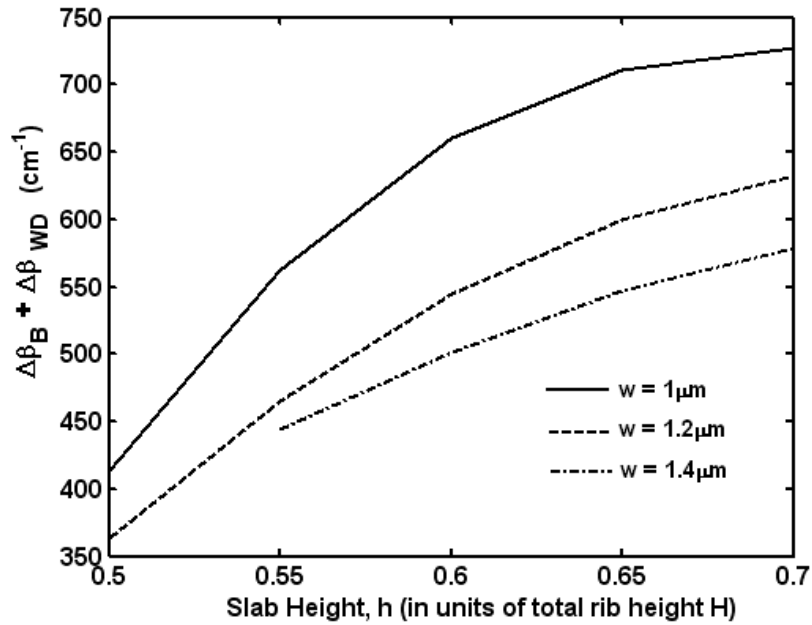

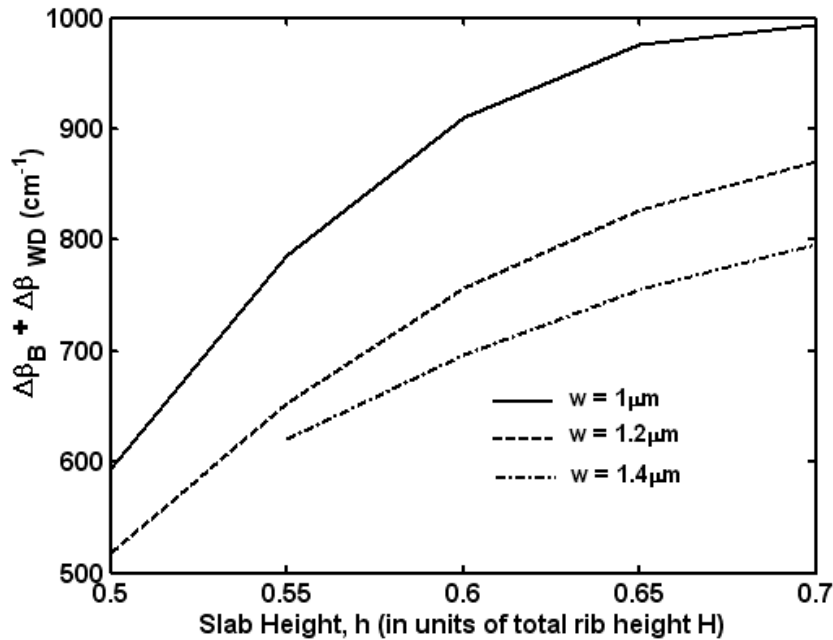Fig. 4. Waveguide induced wavector mismatch for anti-Stokes (1.3348μm) to Stokes (1.55μm) down-conversion.

Fig. 5. Waveguide induced wavevector mismatch for Stokes (1847.9nm) to anti-Stokes (1550nm) up-conversion.

The above trend shows that as we go from $h/H = 0.5$ towards the slab waveguide limit of $h/H = 1$, the mismatch increases. This is due to the fact that this mismatch is dominated by the birefringence which assumes its highest value when the slab geometry is approached (in the other extreme, a square waveguide has zero birefringence).

Adjusting the relative dimensions offers flexibility but for $H = 1.4um$ waveguides the minimum wavevector mismatch achieved with the above variations is ~ 360cm^{-1}. We next consider fixed ratios of $h/H = 0.6$ and $w/H = 1$ and vary w from 2 to 3.5um.
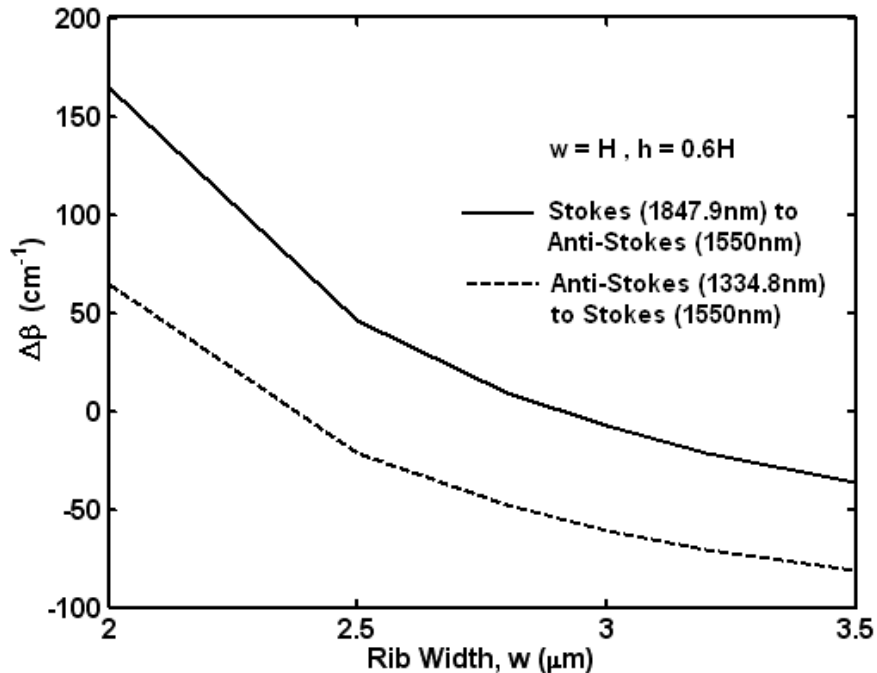
Fig. 6. Total momentum mismatch vs. dimension increase for both Stokes to Anti-Stokes (solid line) and Anti-Stokes to Stokes conversion (dashed line).

The total mismatch (both waveguide and material contributions) as shown in Fig. 6 and drops rapidly as the rib width increases from 2 to 3.5μm. This result is expected and shows that there is an optimum waveguide dimension (around $w = 2.35$μm), where the birefringence and material dispersion will cancel.

The dependence of the phase-mismatch on the pump frequency is also of interest. For a waveguide of dimensions $w = H = 2.3$μm, $h = 0.6H$ the different contributions to the wavevector mismatch and the total mismatch are shown in Fig. 7 for Stokes wavelength between 1500 - 1600nm (pump wavelengths 1391 – 1477nm). Phase-matching is achieved for Stokes wavelength around 1520nm. The calculated waveguide dispersion is ~11cm^{-1}, very low in comparison with the birefringence. We have considered it to be constant over the range of frequencies used. In general, for different waveguide profiles the dispersion is on the order of ~ 5 – 10 cm^{-1}.
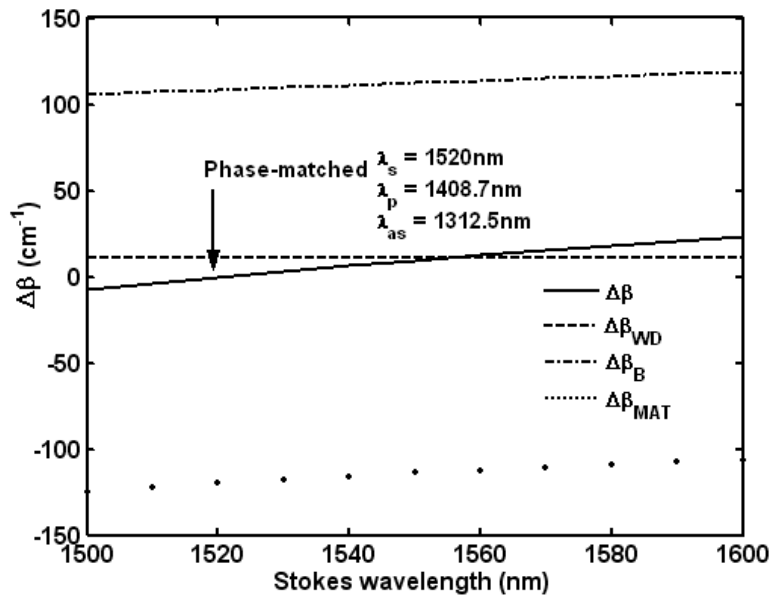
Fig. 7. Momentum mismatch for waveguide $w = H = 2.3\mu m$, $h = 0.6H$ versus Stokes wavelength in CARS : total mismatch (solid line), material dispersion contribution (dotted line), waveguide dispersion contribution (dashed line) and birefringence contribution.

5. Sensitivity to fabrication errors

The above discussion has outlined the technique for achieving phase matching in silicon rib waveguides leading to large wavelength conversion efficiency. Phase matching can be obtained for specific waveguide dimensions. An important issue is the sensitivity of the phase matching condition, and hence the conversion efficiency, to deviations in the rib height and width from the desired values. In practice deviations will occur due to fabrication errors.

Rib waveguides are typically fabricated by using photolithography to define the rib width and Deep Reactive Ion Etching (DRIE) to achieve the desired rib height [1]. Uncertainties in mask dimensions and undercutting during the etching will result in a reduction in the fabricated rib width. A conservative estimate for this reduction is 200nm. Variation in the rib height will result from uncertainty in the actual etch rate. A conservative estimate is +/- 5% of the etch depth. Fig. 8 shows the rib waveguide geometry and possible deviations from the targeted profile.
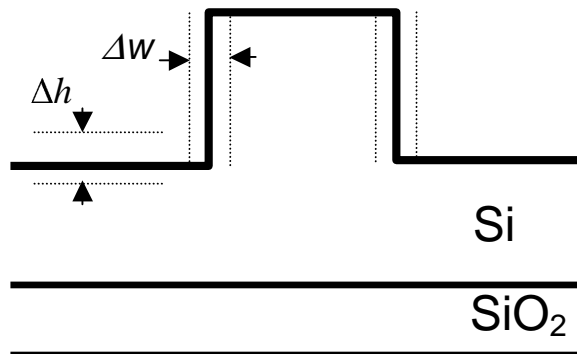

Fig. 8. Waveguide profiles fabricated by LOCOS and DRIE (solid lines) and the targeted profile (dashed line).
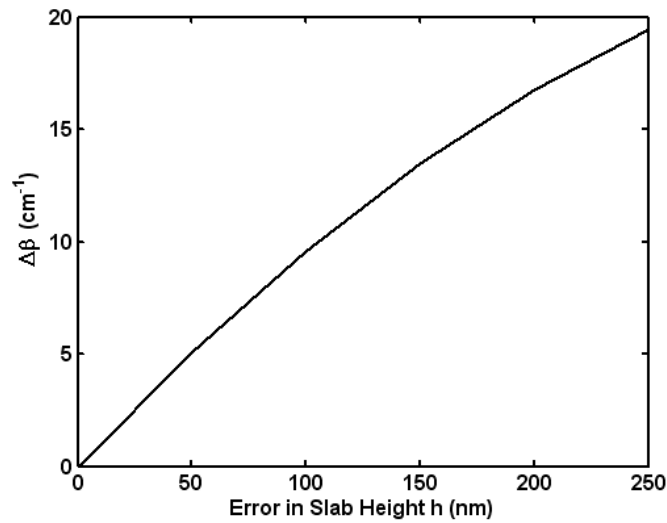
Fig. 9. Phase-mismatch variation with respect to the error in slab height (error in the etching depth) for the phase-matched waveguide w = H = 2.3μm , h = 1.38μm at center wavelength 1520nm.
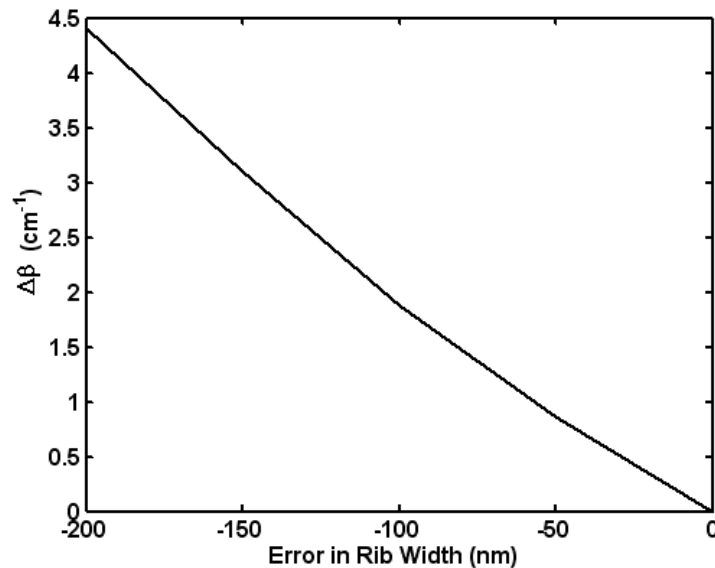

Fig. 10. Phase-mismatch variation with respect to the error in rib width (over-cutting the rib) for the phase-matched waveguide $w = H = 2.3$μm , $h = 1.38$μm at center wavelength 1520nm.

Figures 9 and 10 show the variations of the phase mismatch parameter, $\Delta\beta$, as a function of the variations in rib height Δh and width Δw, respectively. The waveguide considered has $w = H = 2.3$μm and $h = 1.38$μm. The results suggest that in order to maintain the phase mismatch below 1.3 cm^{-1}, the variations in width or etch depth must be less than 70nm and 10nm, respectively. While these are stringent requirements, they are within the capability of silicon manufacturing which is currently producing microprocessors with tens of millions of transistors with 90nm feature size [15]. The tolerance in such processes is typically better than ±5% (i.e., ±4.5nm).

5. Conclusions

The efficiency of FWM arising from Raman and non-resonant nonlinear susceptibilities in silicon waveguides is studied. It is shown that in phase matched waveguides, peak conversion efficiencies of tens of percent can be achieved at pump intensities of $10MW/cm^2$ in a 2cm long waveguide with a loss of 1dB/cm. Group velocity dispersion and birefringence in silicon waveguides was quantified. It was shown the waveguide dispersion and the SPM induced phase mismatch are much smaller than the contributions of the birefringence and the material dispersion, and that phase-matched waveguides can be realized by using the birefringence to compensate for the material dispersion. The sensitivity of the phase matching condition to fabrication error was studied and it was shown that accurate control of rib width and etch depth must be achieved in order to realize a high conversion efficiency.

Acknowledgments